Neurobiology of Disease 178 (2023) 106026

Contents lists available at ScienceDirect

Neurobiology of Disease

journal homepage: www.elsevier.com/locate/ynbdi

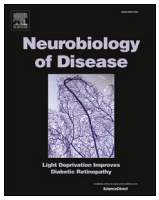

Transient astrocytic accumulation of fluorescein during spreading depolarizations

Karl Schoknecht [a,*], Johannes Hirrlinger [a,b], Jens Eilers [a]

[a] Carl-Ludwig-Institute of Physiology, Medical Faculty, Leipzig University, Leipzig, Germany
[b] Department of Neurogenetics, Max-Planck-Institute for Multidisciplinary Sciences, Göttingen, Germany

ARTICLE INFO

Keywords:
Astrocyte
Fluorescein
Potassium
Spreading depolarization
Swelling

ABSTRACT

Spreading depolarizations (SDs) occur frequently in acute cerebral injuries. They are characterized by a breakdown of transmembrane ion gradients resulting in a reduced extracellular sodium ($[Na^+]_o$) and increased extracellular potassium concentration ($[K^+]_o$). Elevated $[K^+]_o$ induces astrocytic swelling, another feature of SD; however, the solutes that drive astrocytic swelling remain incompletely understood. We incidentally found astrocytic accumulation of fluorescein (Fluo) – a low molecular weight anionic dye – during SDs induced by elevated $[K^+]_o$. Herein, we aimed to explore the properties of astrocytic Fluo accumulation during SDs, electrical stimulation, $[K^+]_o$ and glutamate elevation and elucidate underlying mechanisms and its relation to swelling. Experiments were performed in acute neocortical slices from adult male C57Bl6 mice and transgenic mice expressing tdTomato in parvalbumin (PV)-positive neurons. We labeled astrocytes with sulforhodamine-101 (SR-101), measured Fluo kinetics using 2-photon laser scanning microscopy and recorded local field potentials (LFP) to detect SDs. Elevations of $[K^+]_o$ lead to an increase of the astrocytic Fluo intensity in parallel with astrocytic swelling. Pharmacological inhibitors of sodium-potassium ATPase (Na/K-ATPase), secondary-active transporters and channels were used to address the underlying mechanisms. Fluo accumulation as well as swelling were only prevented by inhibition of the sodium-potassium ATPase. Application of glutamate or hypoosmolar solution induced astrocytic swelling independent of Fluo accumulation and glutamate opposed Fluo accumulation when co-administered with high $[K^+]_o$. Astrocytes accumulated Fluo and swelled during electrical stimulation and even more during SDs. Taken together, Fluo imaging can be used as a tool to visualize yet unidentified anion fluxes during $[K^+]_o$- but not glutamate- or hypoosmolarity induced astrocytic swelling. Fluo imaging may thereby help to elucidate mechanisms of astrocytic swelling and associated fluid movements between brain compartments during physiological and pathological conditions, e.g. SDs.

List of abbreviations

4-CIN	alpha-cyano-4-hydroxycinnamic acid
AC	alternate current
$BaCl_2$	barium chloride
DC	direct current
DCPIB	4-[(2-butyl-6,7-dichloro-2-cyclopentyl-2,3-dihydro-1-oxo-1*H*-inden-5-yl)oxy]butanoic acid
DIDS	4,4′-diisothiocyanostilbene-2,2′-disulfonic acid
DL-TBOA	DL-*threo*-β-benzyloxyaspartic acid)
DMSO	dimethyl sulfoxide
EAAT	excitatory amino acid transporter
Fluo	Fluorescein
GLUT-1	glucose transporter 1
$[K^+]_o$	extracellular potassium
Kir4.1	inward-rectifier potassium channel 4.1
IQR	interquartile range
MCT	monocarboxylate transporter
$[Na^+]_o$	extracellular sodium
Na/K-ATPase	sodium-potassium ATPase
n.s.	not significant
OATP	organic anion transporting polypeptide
PV	parvalbumin
ROI	region of interest
SD	spreading depolarization
SR 101	Sulforhodamine-101;
TFB-TBOA	

(*continued on next column*)

(*continued*)

(*continued on next page*)

* Corresponding author at: Carl-Ludwig-Institute of Physiology, Medical Faculty, Leipzig University, Liebigstr. 27, 04103 Leipzig, Germany.
E-mail address: karl.schoknecht@medizin.uni-leipzig.de (K. Schoknecht).

https://doi.org/10.1016/j.nbd.2023.106026
Received 23 August 2022; Received in revised form 16 January 2023; Accepted 29 January 2023
Available online 31 January 2023

(*continued*)

	((3*S*)-3-[[3-[[4-(trifluoromethyl)benzoyl]amino]phenyl]meth-oxy]-L-aspartic acid
ttx	tetrodotoxin

1. Introduction

Spreading depolarizations (SDs) are characterized by a near-complete breakdown of transmembrane ion gradients and propagate at 2–8 mm/min through the cortex. SDs have been associated with acute cerebral injuries, e.g. traumatic brain injury, ischemic and hemorrhagic stroke, but also with migraine aura (Dreier and Reiffurth, 2015). Animal and human studies suggest that SDs contribute to injury progression when concomitant extra energy demand to restore ion gradients can no longer be met by cerebral perfusion (Lemale et al., 2022).

SDs are characterized by a negative direct current (DC) potential deflection, flattening of alternate current (AC) recordings indicative for depression of neuronal firing in electrically active tissue, increased extracellular potassium ($[K^+]_o$) (Dreier et al., 2017), and swelling of neurons and astrocytes, i.e. cytotoxic edema (Zhou et al., 2010; Risher et al., 2012; Dreier et al., 2018). In addition to cytotoxic edema, SDs were shown to increase blood-brain barrier (BBB) permeability (Gursoy-Ozdemir et al., 2004; Sadeghian et al., 2018; Parker et al., 2022), which may cause vasogenic edema.

Sodium fluorescein is a marker to measure BBB permeability. It is commonly applied intravenously and indicates *blood-to-brain* 'leakage' when detected in the extravascular compartment (Schoknecht et al., 2014). In aqueous solution sodium fluorescein dissociates. Fluorescein (abbreviated Fluo in the following; molecular weight: 332 Da) is thus a negatively charged solute. In pilot experiments in acute brain slices, we applied Fluo extravascularly to study its transport from *brain-to-blood* during K^+-induced SDs. Unexpectedly, we noticed transient Fluo 'brightening' of a subpopulation of cells that turned out to be astrocytes. This led us to identify triggers of astrocytic Fluo accumulation, explore underlying mechanisms and test if Fluo indicates astrocytic water influx. Candidate triggers for Fluo accumulation and water influx are extracellular $[K^+]_o$ and glutamate. Both rise during SDs (Lemale et al., 2022) and have caused astrocytic swelling (Hansson et al., 2000; Risher et al., 2009; Florence et al., 2012; Larsen and MacAulay, 2017; Shi et al., 2017; Walch et al., 2020). Still, the specific solute fluxes that ultimately attract water remain incompletely understood (Dreier et al., 2018).

Using 2-photon imaging and local field potential recordings in acute mouse brain slices, we show that Fluo serves as a marker for K^+- but not glutamate- or hypoosmolarity induced astrocytic swelling during stimulated activity and SD. Elucidating Fluo kinetics during SD may lead to a better understanding of the role of astrocytes during the formation of cytotoxic and vasogenic edema and the underlying bulk fluid movements.

2. Material and methods

Animals were housed and bred in accordance with the German Animal Welfare Act and the European Communities Council Directive (2010/63/EU) with approval of the local authorities (T10/20, TVV74/21). This study included 48 adult (11–24 week-old) male C57Bl6 mice and two 5–9 week-old male transgenic PV-tdTomato mice. To create transgenic PV-tdTomato animals, the Cre-reporter mouse line Ai14 (Madisen et al., 2010) expressing TdTomato (Shaner et al., 2004) was recombined with the PV^{CRE} knockin-mice expressing Cre-recombinase exclusively in PV-positive interneurons (The Jackson Laboratory, stock no. 017320).

2.1. Preparation

All experiments were conducted in acute neocortical brain slices. Following brief anesthesia by isoflurane, animals were decapitated, brains were removed and cut into coronal slices (thickness 300 μM) on a vibratome (Leica VT1200S, Leica Biosystems, Nussloch, Germany) in ice-cooled artificial cerebrospinal fluid (aCSF). Thereafter slices were kept in warmed aCSF (35 °C) for 30 min before being transferred to room temperature (20–22 °C). Fluo (0.1–0.5 μM, fluorescein sodium salt, Merck, Darmstadt, Germany) and sulforhodamine 101 (SR-101, 130–275 nM, Sigma Aldrich) were added to the aCSF from water-dissolved stock solutions (0.1 and 1 mg/ml for Fluo and SR-101 respectively) immediately after slicing. Slices from PV-tdTomato mice were incubated with Fluo only.

2.2. Solutions and drugs

Drugs were purchased from Sigma Aldrich if not stated otherwise. ACSF contained in mM: 125 NaCl, 2.5 KCl, 1.25 NaH_2PO_4, 26 $NaHCO_3$, 1.8 $MgCl_2$, 2 $CaCl_2$, and 20 glucose and was continuously carbogenated in 95% oxygen 5% CO_2 (pH 7.4, osmolarity ~305 mOsm). In aCSF containing higher concentrations of KCl (up to 20 mM), NaCl was replaced with KCl to maintain constant osmolarity. NaCl-free aCSF contained in mM: *N*-methyl-D-glucamine (NMDG, 105 mM), HEPES (10 mM), 2.5 KCl, 1.2 NaH_2PO_4, 30 $NaHCO_3$, 1.8 $MgCl_2$, 2 $CaCl_2$, and 20 glucose. K^+ concentrations were increased to 10 mM by isosomolar exchange of KCl with NMDG. Other chemicals: alpha-cyano-4-hydroxycinnamic acid (4-CIN, 200 μM), barium chloride dihydrate ($BaCl_2$, 100 μM-3 mM), cytochalasin B (20 μM), DCPIB (10 μM, 4-[(2-butyl-6,7-dichloro-2-cyclopentyl-2,3-dihydro-1-oxo-1*H*-inden-5-yl)oxy] butanoic acid, both Tocris Bioscience, Bristol, UK), digoxin (10 μM), dimethyl sulfoxid (<0.1%, DMSO), glutamic acid monosodium salt (0.2–1 mM), ouabain octahydrate (10 μM), phloretin (100 μM), probenecid (400 μM), S0859 (30 μM), DL-TBOA (DL-*threo*-β-benzyloxyaspartic acid, 50 μM), TFB-TBOA ((3*S*)-3-[[3-[[4-(trifluoromethyl) benzoyl]amino]phenyl]methoxy]-L-aspartic acid, 200 nM), and tetrodotoxin (ttx, 0.5–1 μM, last three from Tocris Bioscience).

2.3. Microscopy

For imaging and parallel electrophysiological recordings, slices were transferred to an open bath perfusion chamber (Warner Instruments, Holliston, MA, USA, perfusion rate 6–8 ml/min). To prevent movement artifacts slices were mounted with a U-shaped platinum wire holding a nylon grid. Images were acquired by 2-photon laser scanning microscopy (excitation at 800 nm) using a Ti:Sapphire laser (Mai Tai DeepSee, Spectra-Physics, Milpitas, CA, USA) and a laser scanning microscope (Olympus Fluoview 10 M, Olympus, Tokyo, Japan) equipped with a 25× objective (XLPlan N 25× W NA:1.05, Olympus) controlled by Olympus Fluoview ASW (Version 04.01) software. Fluorescence was low pass filtered (690 nm) before passing a dichroic mirror (D570 nm). The two resulting channels were further bandpass filtered with 495–540 nm and 575–630 nm barrier filters (for 'green' Fluo and 'red' SR-101 signal, respectively). Images were acquired as xyz-time series with zoom factor 2–5 (image dimension 128 × 128 to 512 × 512 pixels, xy-pixel-dimension 0.2–1 μm), up to 25 z-steps at intervals of 1–1.5 μm and time intervals between 15 s (stimulation and spreading depolarization (SD)) and 2 min (K^+ and/or drug wash-in and washout). To analyse the propagation of SDs, we measured light transmission in a third channel as previously described (Dreier et al., 2018) and the field of view was enlarged using a 10× objective (UMPLanFl 10× W NA:0.30) (single z-plane, zoom factor 1, x&y = 2.5 μm/pixel, t = 2.5 s).

2.4. Electrophysiological recordings

Local field potentials (LFP) were recorded ~50 μm below the surface

of the slice using microelectrodes prepared in-house from borosilicate glass (Science Products, Hofheim, Germany, pipette puller PC-10, Narishige, Tokyo, Japan). The LFP signal was amplified (EXT-10), low-pass filtered (3 kHz, LPBF-01GX, both npi electronic, Tamm, Germany) and digitized (HEKA patch clamp EPC10 with PatchMaster v2x90.2 software, HEKA Elektronik or CED-1401 Micro3 with Spike2 9.01 software, Cambridge Electronic Design, Cambridge).

2.5. Electrical stimulation and induction of SD

Monopolar electrical stimulation was achieved with glass microelectrodes (same as for LFP recording) and a stimulus isolator (ISO-STIM 01M, npi electronic) triggered by the patch clamp amplifier. A full-length stimulation series consisted of 18 bursts given at 0.1 Hz with each burst consisting of 50 pulses (1 ms, 25–60 V) given at 10 Hz. The stimulation electrode was placed at the border of white and gray matter and the recording electrode was placed in layer 2–3. SDs were induced focally using glass microelectrodes (see above) containing KCl (3 M), which was released by a manually-triggered system for applying pressured air (0.5 bar, PDES-2L, npi electronic).

2.6. Experimental protocols

All experiments began with a baseline recording consisting of 3 consecutive xyz-stacks at $[K^+]_o$ 2.5 mM. All wash in experiments (i.e. of increasing concentrations of $[K^+]_o$, $[K^+]_o$ in combination with drugs, glutamate or hyposomotic aCSF) lasted for 5 xyz-stacks (i.e. 10 min wash in) and the last stack was used for quantifying astrocytic area and Fluo intensity (see below 'data analysis'). Astrocytic area and Fluo intensity after wash in of $[K^+]_o$ 10 mM for 10 min served as a slice-internal reference for effects of drugs, glutamate (0.2–1 mM) and 30% hypoosmotic aCSF.

During stimulation and SD (see induction protocol above), imaging was continued for at least 3 min after stimulation and until complete repolarization after the SD. In a subset of slices, two stimulation series were conducted, one in drug-free aCSF and one in aCSF containing ttx (0.5–1 μM). The sensitivity of SD-associated astrocytic area and Fluo changes to ouabain (10 μM) were investigated by comparing one SD evoked after bath application of aCSF containing ouabain (~10 min wash in) to a previous SD evoked in drug-free aCSF in the same slice. Area and Fluo quantification during stimulation and SD are averages at maximum ±1 acquisition timepoint.

2.7. Data analysis

All data were analyzed in Matlab (The MathWorks, Natick, Ma, USA, version R2019b). SDs were detected by eye. To quantify astrocytic area and Fluo intensity, xyz-time series were converted to maximum-intensity z-projection time series. Background was assessed by recording photomultiplier (PMT) signals at employed offset and gain settings *without* laser excitation and was subtracted. XY-movements were corrected using the *dftregistration* algorithm (Guizar-Sicairos et al., 2008). To segment astrocytes, SR-101 images underwent a gaussian low pass filter (Matlab function: 'fspecial') before being turned into binary images by mean-based thresholding (mean + doubled standard deviation). Two to three astrocytes per field of view were individually selected with rectangular regions of interest (ROI), and the binary images (pixels showing a SR-101 signal) were used to quantify the astrocytic area by summing up the number of pixels within the ROI and to quantify the median Fluo intensity for the SR-101-positive pixels. These time-dependent values were self-normalized to baseline. Values of individual astrocytes were averaged per slice and then referred to as $n = 1$.

Changes in light transmission (T) were calculated as a relative change. The last baseline image prior to SD induction was subtracted from all subsequent images and the calculated differences were normalized to the absolute baseline transmission and expressed in %.

2.8. Data reporting and statistical analysis

This is an exploratory study. Due to the lack of prior evidence sample sizes could not be accurately estimated and were selected to comply with likewise research. Slices were excluded from analysis if movement artifacts prevented reliable analysis and if stimulation or SD-induction were ineffective. Data are reported as median and interquartile range (IQR). Boxes in boxplots display median, 25th and 75th percentile (lower and upper box limit, respectively). Whiskers extend to minimal and maximal values unless considered as outliers ('+', values >1.5*IQR). Data analysis was automated once rectangular ROIs around astrocytes were selected, but not blinded. Statistical inference was performed by Wilcoxon test for paired comparisons and Bonferroni correction for multiple comparisons. Differences were considered significant at $p < 0.05$. Data will be made available upon reasonable request.

3. Results

3.1. Astrocytic Fluo accumulation and volume depend on $[K^+]_o$

We incidentally observed that astrocytes accumulate Fluo during SDs induced by 20 mM $[K^+]_o$ in acute mouse brain slices. To investigate whether Fluo accumulation depends on $[K^+]_o$, we applied increasing concentrations of $[K^+]_o$ through isosomotic exchange of KCl for NaCl in the aCSF. All slices developed SDs at either 15 mM or 20 mM $[K^+]_o$. In line with previous reports (Risher et al., 2009; Florence et al., 2012; Walch et al., 2020), stepwise elevation of $[K^+]_o$ from 2.5 to 20 mM increased the astrocyte-covered area (Fig. 1A-D) proportionally by 60% (40, 78) (median (IQR), $n = 14$ cells, 5 slices, 2 mice) at 20 mM $[K^+]_o$ compared to baseline ($[K^+]_o$ 2.5 mM), which approximately corresponds to volume doubling. In parallel, astrocytic Fluo intensity increased with each step and reached up to factor 2.3 (2.11, 2.38) (Fig. 1B,D). In contrast to Fluo, SR-101 intensity decreased during astrocytic swelling (Fig. 1C), probably due to the dilution of SR-101 during the swelling of astrocytes. Using the PV-tdTomato reporter mouse line, we found that PV-positive neurons did not accumulate Fluo, while putative astrocytes showed the typical increase in Fluo intensity during bath application of $[K^+]_o$ (Fig. 1E,F).

3.2. Astrocytic Fluo accumulation is a hallmark of K^+ induced swelling

To investigate whether Fluo accumulation is exclusive to elevations in $[K^+]_o$ or is a general marker of astrocytic swelling, we measured the kinetics of Fluo during K^+-, glutamate-induced, and osmotic swelling (Fig. 2). As expected, the astrocytic area increased in response to all three stimuli, namely by 19% (16, 28), 24% (17, 38) and 18% (13,20) during wash in of $[K^+]_o$ 10 mM ($n = 18$ slices, 12 mice), glutamate 0.2–1 mM ($n = 11$ slices, 6 mice), and 30% hypoosmotic aCSF ($n = 7$ slices, 6 mice), respectively ($p < 0.001$, $p = 0.003$, and $p = 0.047$, respectively, Wilcoxon tests and Bonferroni correction, Fig. 2E). While Fluo intensity increased by factor 1.43 (1.34, 1.57) at $[K^+]_o$ 10 mM, it decreased by factor 0.91 (0.83, 0.97) and 0.87 (0.83, 0.93) during bath application of glutamate and hypoosmolar aCSF, respectively ($p < 0.001$, $p = 0.006$, $p = 0.094$, Wilcoxon tests and Bonferroni correction, Fig. 2E). Taken together, our data imply that astrocytic Fluo accumulation accompanies K^+-induced swelling, but is not a marker of glutamate-induced or osmotic astrocytic swelling.

3.3. Na/K-ATPase inhibition prevents astrocytic Fluo accumulation

Na/K-ATPase inhibition was shown to prevent astrocyte-selective K^+-induced swelling in acute brain slices (Walch et al., 2020), while the solutes that ultimately drive swelling remain largely unknown. We

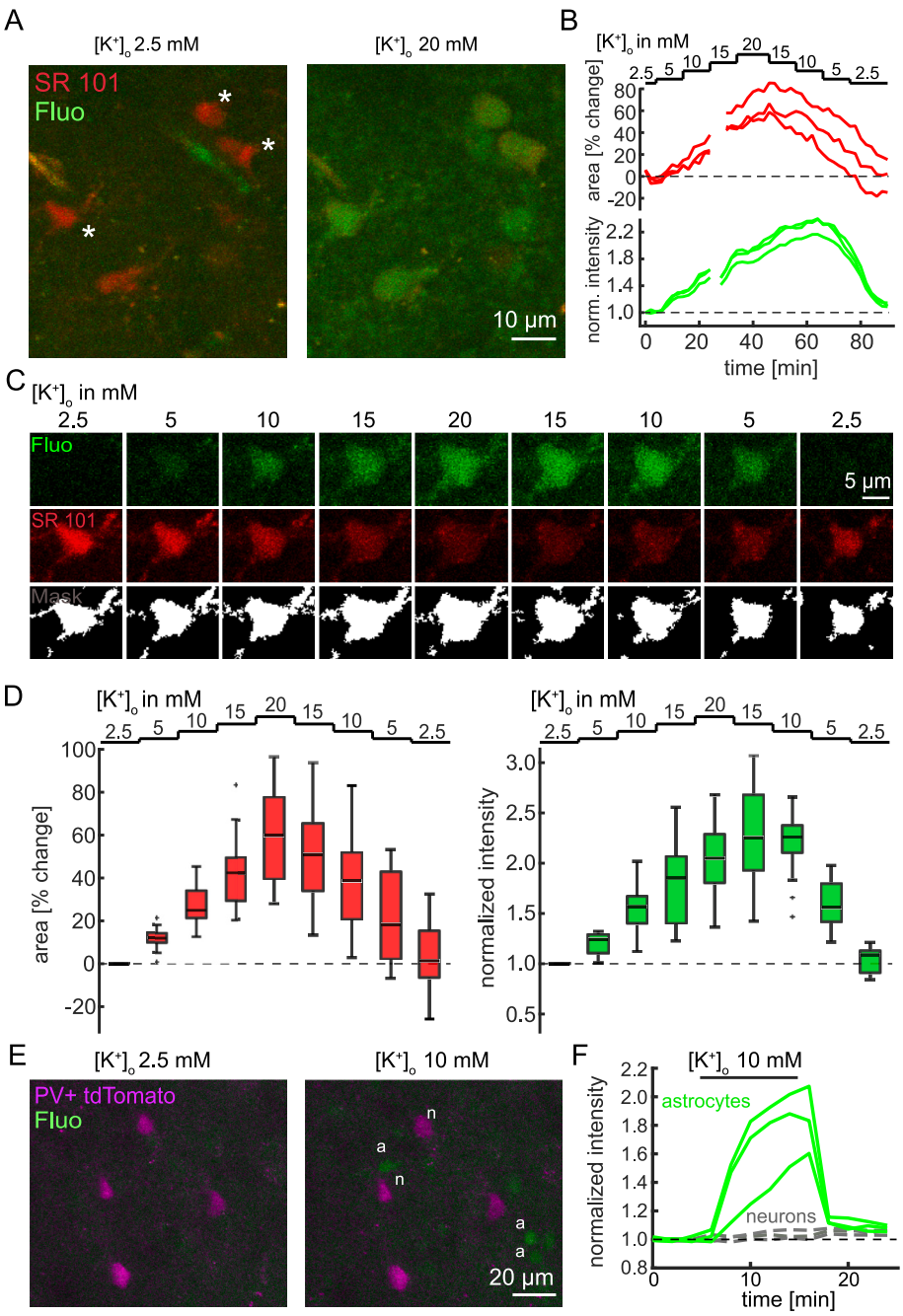

Fig. 1. Astrocytes take up Fluo and swell when $[K^+]_o$ is elevated.
A) Two-colour z-projections (25 planes taken at 1 µm interval) of a mouse neocortical brain slice after staining with the astrocytic marker sulforhodamine 101 (SR-101, 0.1 µM, red) and in the continuous presence of 0.5 µM sodium fluorescein (green). Left, control conditions, asterisks denote astrocytes analyzed in B and C. Right, images taken 10 min into bath application of 20 mM KCl. Note that the SR-101 pixel intensity decreases due to substantial cell swelling (cf. C) while the Fluo intensity increases due to dye accumulation.
B) Dose-response curves of the area (calculated from the number of pixels with SR-101 signal, cf. C) and the Fluo intensity (both self-normalized to the control measurement at 2.5 mM K^+) for the three astrocytes indicated in A. The gap in the traces is due to a spreading depolarization (SD), which prevented image analysis at these time points due to the temporary drift in the z-axis. SDs were induced in all slices (cf. D) at concentrations ≥15 mM $[K^+]_o$.
C) Exemplary recording from the left-most astrocyte marked in A. Stepwise increases in $[K^+]_o$ induced proportional increases of the Fluo intensity (top row). In contrast, SR 101 intensity (middle row) decreased due to increased cell volume (segmented images, bottom row, 'Mask'). Note that these effects were reversible upon stepwise decreases in $[K^+]_o$.
D) Summarizing box plots of the increase in area and in Fluo signal (left and right, respectively; $n = 14$ astrocytes, 5 slices, 2 mice). Data are normalized to the control measurement at 2.5 mM $[K^+]_o$; outliers are shown as'+'.
E) Two-colour imaging as in A but in a slice from a mouse expressing tdTomato in parvalbumin-positive (PV+) neurons and without SR 101 staining. Left, control condition (2.5 mM $[K^+]_o$), right, 10 min after perfusion of 10 mM $[K^+]_o$, astrocytes and PV^+ neurons are marked by 'a' and 'n', respectively.
F) Fluo signal intensity in astrocytes and neurons (solid and dashed lines, respectively) marked in E during bath application of 10 mM $[K^+]_o$. Note that neurons did not take up significant amounts of Fluo in response to elevated $[K^+]_o$. (For interpretation of the references to colour in this figure legend, the reader is referred to the web version of this article.)

therefore tested if accumulation of the anion Fluo is coupled to Na/K-ATPase-sensitive swelling of astrocytes. Confirming previous experiments (Walch et al., 2020), ouabain (10 µM, Na/K-ATPase inhibitor) reduced the increase in astrocytic area during bath application of $[K^+]_o$ 10 mM (compared with $[K^+]_o$ 2.5 mM) from 18% (16, 22) to 4% (0, 8) (Fig. 3 A,B). In parallel, ouabain reduced the increase in Fluo intensity from 1.54 (1.41, 1.59) to 0.95 (0.85, 1.00; $n = 10$ slices, 4 mice, Wilcoxon test, both: $p = 0.002$, Fig. 3 A,B). The effects of ouabain were corroborated using digoxin (10 µM, inhibitor of Na/K-ATPase), which reduced the astrocytic increase in Fluo intensity during $[K^+]_o$ 10 mM wash in from factor 1.69 (1.44, 1.70) to 1.05 (1.03, 1.12) and reduced the increase in area from 14% (12, 19) to 3% (0, 4), respectively ($n = 6$ slices, 3 mice, both: $p = 0.016$, Wilcoxon test, Fig. 3C and Supplementary Fig. 1A). We next tested if K^+-induced astrocytic Fluo accumulation depends on the extracellular sodium concentration ($[Na^+]_o$), comparing wash in of $[K^+]_o$ 10 mM in standard aCSF to NaCl-free aCSF. The NaCl-free aCSF contains 31 mM Na^+ due to other sodium salts within the aCSF. Similar to Na/K-ATPase inhibition, low $[Na^+]_o$ reduced the increase in K^+-induced Fluo intensity from factor 1.60 (1.31,1.70) to 1.14 (1.07, 1.19) and also reduced swelling (increase in area reduction from 23% (17, 26) to 3% (3, 7; $n = 7$ slices, 3 mice, both: $p = 0.016$, Wilcoxon test, Fig. 3D and Supplementary Fig. 1B). To summarize, our data implies that K^+-induced astrocytic Fluo accumulation and swelling depend on Na/K-ATPase function and $[Na^+]_o$.

3.4. Pharmacological profile of Fluo accumulation and role for swelling

To elucidate specific mechanisms of K^+-induced astrocytic Fluo accumulation, we examined several pharmacological inhibitors of secondary-active transporters and channels. As a reference, the effect of ouabain is again displayed in Fig. 3E as a relative change of area and intensity comparing the effect of '10 mM $[K^+]_o$ + drug' to '10 mM $[K^+]_o$'

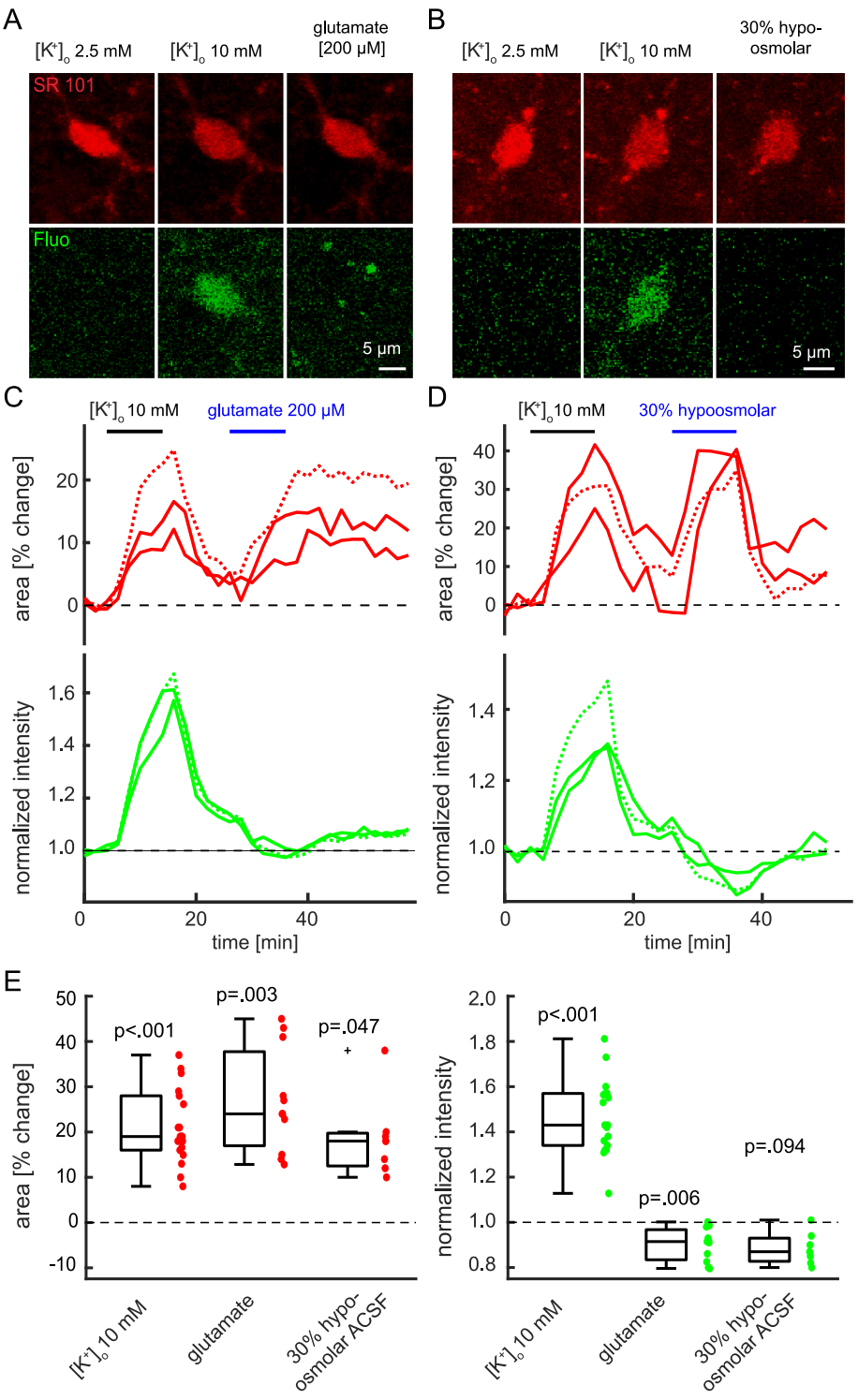

Fig. 2. Astrocytes accumulate Fluo during K^+- but not glutamate-induced or osmotic swelling.
A) SR 101 (red, top) and Fluo (green, bottom) z-projection images of an astrocyte in a neocortical brain slice. Left, control condition ($[K^+]_o$ 2.5 mM), middle, 10 min after wash in of 10 mM $[K^+]_o$ and, right, 10 min after wash out of high K^+, followed by 10 min wash in of 200 µM glutamate. Fluo (0.5 µM) was continuously present in the aCSF.
B) Two-colour imaging as in A. Left, control condition ($[K^+]_o$ 2.5 mM), middle, 10 min after wash in of 10 mM $[K^+]_o$, and right, 10 min after wash out of high K^+, followed by 10 min wash in of 30% hypoosmolar aCSF.
C) Self-normalized area (red) and Fluo intensity (green) in three astrocytes during temporary wash in of 10 mM $[K^+]_o$ and of 200 µM glutamate. The dotted traces correspond to the astrocyte shown in A.
D) Self-normalized area (red) and Fluo intensity (green) during temporary perfusion of 10 mM $[K^+]_o$ and of 30% hypoosmolar aCSF. The dotted traces correspond to the astrocyte shown in B.
E) Boxplots of astrocytic area (left) and Fluo intensity (right) after bath application of $[K^+]_o$ 10 mM, glutamate (200 µM and 1 mM, pooled data), and 30% hypoosmotic aCSF for 10 min (each normalized to control ($[K^+]_o$ 2.5 mM)). $[K^+]_o$ 10 mM: $n = 18$ slices, 12 mice; glutamate: 200 µM: $n = 4$ slices, 2 mice, 1 mM $n = 7$ slices, 5 mice; hyposmolar aCSF n = 7 slices, 6 mice; Wilcoxon test and Bonferroni correction, outlier is shown as '+'. (For interpretation of the references to colour in this figure legend, the reader is referred to the web version of this article.)

alone (Fig. 3E, most left box in either boxplot). 0% relative change refers to no change in area or Fluo intensity despite 10 mM $[K^+]_o$ (i.e. complete prevention of swelling or Fluo accumulation by the drug; Fig. 3A) and 100% indicates no drug effect. Neither inhibition of excitatory amino acid transporters (EAAT1–3, inhibitors: DL- and TFB-TBOA, 50 µM and 200 nM), of sodium-bicarbonate exchanger-1 (NBCE-1, S0859, 30 µM), of organic anion transporter polypeptides (OATPs, probenecid, 400 µM), of monocarboxylate transporters (MCTs, phloretin, 100 µM, or 4-CIN, 200 µM), of glucose transporter 1 (GLUT1, cytochalasine B, 20 µM), of inward-rectifier K^+ channel 4.1 (Kir4.1, barium chloride, 100 µM), nor of volume-regulated anion channels (VRAC, DCPIB, 10 µM), reduced astrocytic swelling or Fluo accumulation (Fig. 3E). Taken together, while NaK-ATPase inhibition reduced both K^+-induced astrocytic swelling as well as Fluo accumulation, none of the targeted solitary transporters or channels had a similar effect.

3.5. *Glutamate prevents astrocytic Fluo accumulation but not swelling*

We found that inhibition of astrocytic glutamate uptake (through inhibition of EAATs) did not prevent the increase of astrocytic Fluo

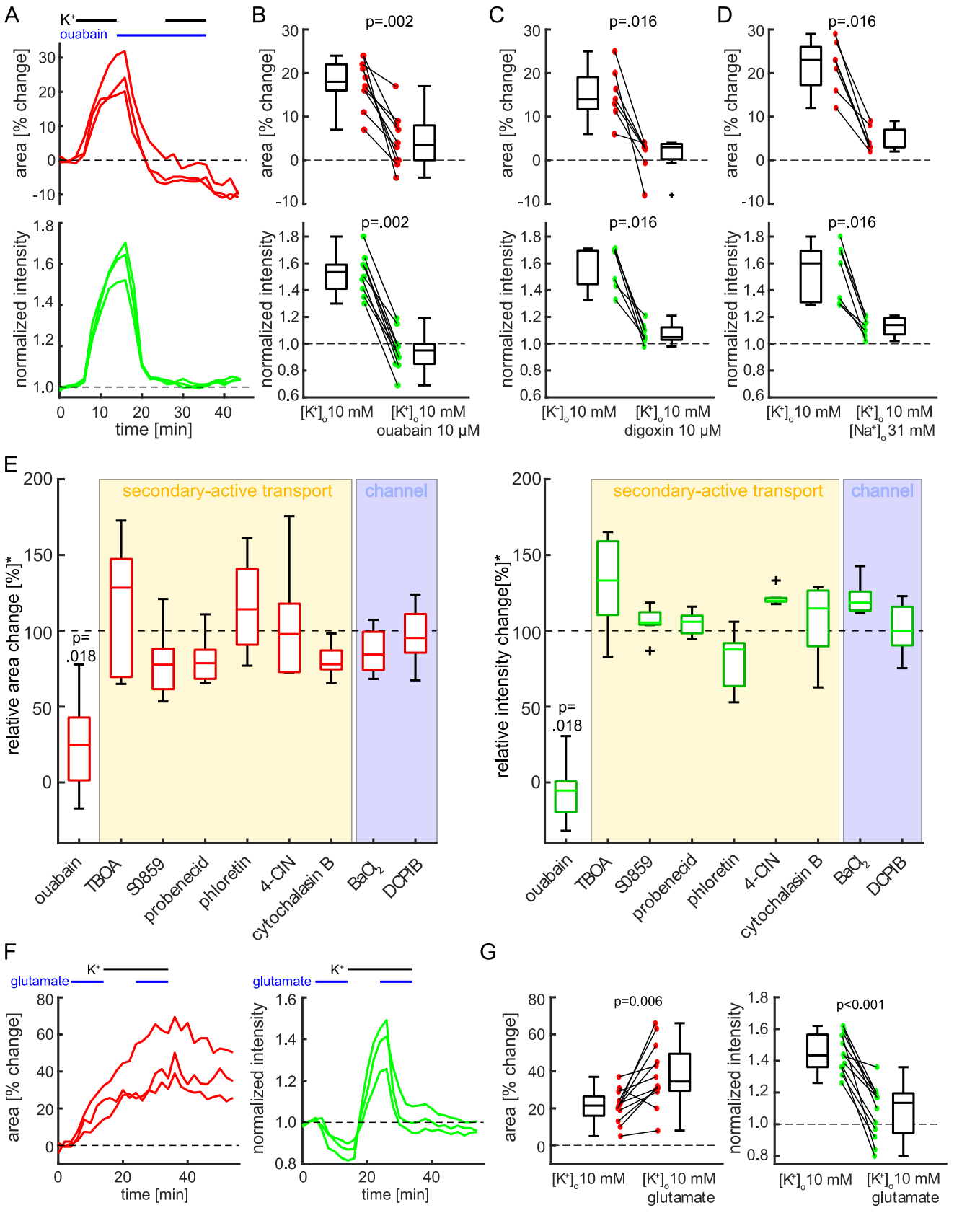

(caption on next page)

Fig. 3. Pharmacological profile of Fluo accumulation and swelling.
A) Self-normalized area (top) and Fluo intensity (bottom) in three astrocytes from a neocortical slice upon wash-in of high K^+ before and during application of the Na/K-ATPase inhibitor ouabain (10 μM). Note that ouabain prevented both swelling and Fluo accumulation.
B) Boxplots of self-normalized area (top) and Fluo intensity for Na/K-ATPase inhibition by 10 μM ouabain (top and bottom, respectively; $n = 10$ slices, 4 mice, Wilcoxon test).
C) Boxplots summarizing data for Na/K-ATPase inhibition by 10 μM digoxin (n = 7 in 6 slices, 3 mice, Wilcoxon test). Exemplary traces are shown in Supplementary Fig. 1A.
D) Boxplots comparing K^+-induced changes in astrocytic area and Fluo accumulation in aCSF containing physiological $[Na^+]_o$ to aCSF wherein Na^+ was partly replaced by NMDG (n = 7 slices, 3 mice, Wilcoxon test). Exemplary traces are shown in Supplementary Fig. 1B.
E) Summarizing boxplots for drug effects on K^+-induced changes in astrocytic area (left) and Fluo intensity (right). Drugs targeted the Na/K-ATPase as well as secondary-active transporters and channels (yellow and blue rectangle respectively). Relative change (in %) = percent change during *high* $[K^+]_o$ *& drug* over percent change during *high* $[K^+]_o$. 0% indicates a complete block with absence of swelling and/or Fluo accumulation induced by 10 mM $[K^+]_o$ and 100% indicates full swelling and/or Fluo accumulation and no drug effect. Ouabain (10 μM, $n = 10$ slices, 4 mice (as shown also in B); TBOA (DL-TBOA, 50 μM, n = 7 slices, 3 mice and TFB-TBOA, 200 nM, $n = 3$ slices, 2 mice), inhibitors of excitatory-amino acid (EAAT) transport; S0859 (30 μM, n = 7 slices, 3 mice), inhibitor of sodium-bicarbonate exchanger – 1 (NBCE-1); probenecid (400 μM, $n = 5$ slices, 2 mice), organic anion transporter inhibitor; phloretin (100 μM, $n = 6$ slices, 3 mice) & 4-CIN (200 μM, n = 6 slices, 2 mice), monocarboxylate-transporter inhibitors; cytochalasin B (20 μM, n = 5 slices, 2 mice), glucose transporter-1 inhibitor; BaCl (barium chloride (100 μM, n = 6 slices, 3 mice), blocker of inward-rectifier potassium channels; DCPIB (10 μM, n = 6 slices, 2 mice), inhibitor of volume-regulated anion channels. Wilcoxon test and Bonferroni correction, *p*-values are written above bars when <0.05, i.e. when a given drug significantly altered area or fluoresence after bath application of 10 mM $[K^+]_o$ compared to the slice-internal reference (bath application of 10 mM $[K^+]_o$ without a drug). Note that only ouabain significantly reduced astrocytic swelling and Fluo accumulation.
F) Exemplary graphs (3 astrocytes from one brain slice) of self-normalized area and Fluo intensity during sequential perfusion of 200 μM glutamate and 10 mM $[K^+]_o$ individually and in combination. Note that glutamate reduced the astrocytic Fluo intensity in the presence of 10 mM $[K^+]_o$.
G) Boxplots summarizing changes in astrocytic area (left) and Fluo accumulation (right) after 10 min perfusion of 10 mM $[K^+]_o$ and of 10 mM $[K^+]_o$ combined with glutamate ($n = 12$ slices, 5 mice, Wilcoxon-test). Glutamate data at concentrations of 200 μM and 1 mM were pooled (n = 7 & 5 slices, from 3 and 2 mice, respectively). (For interpretation of the references to colour in this figure legend, the reader is referred to the web version of this article.)

intensity during bath application of $[K^+]_o$ 10 mM. Conversely, we saw a trend towards increased astrocytic Fluo accumulation during EAAT inhibition (Fig. 3E). To investigate, whether this effect is due to extracellular accumulation of glutamate, we measured astrocytic Fluo intensity and area during bath application of $[K^+]_o$ 10 mM and compared it to aCSF containing $[K^+]_o$ 10 mM and glutamate (0.2–1 mM). In contrast to EAAT inhibition, the additional glutamate reduced Fluo intensity from factor 1.43 (1.36, 1.57) to 1.13 (0.95, 1.20) and

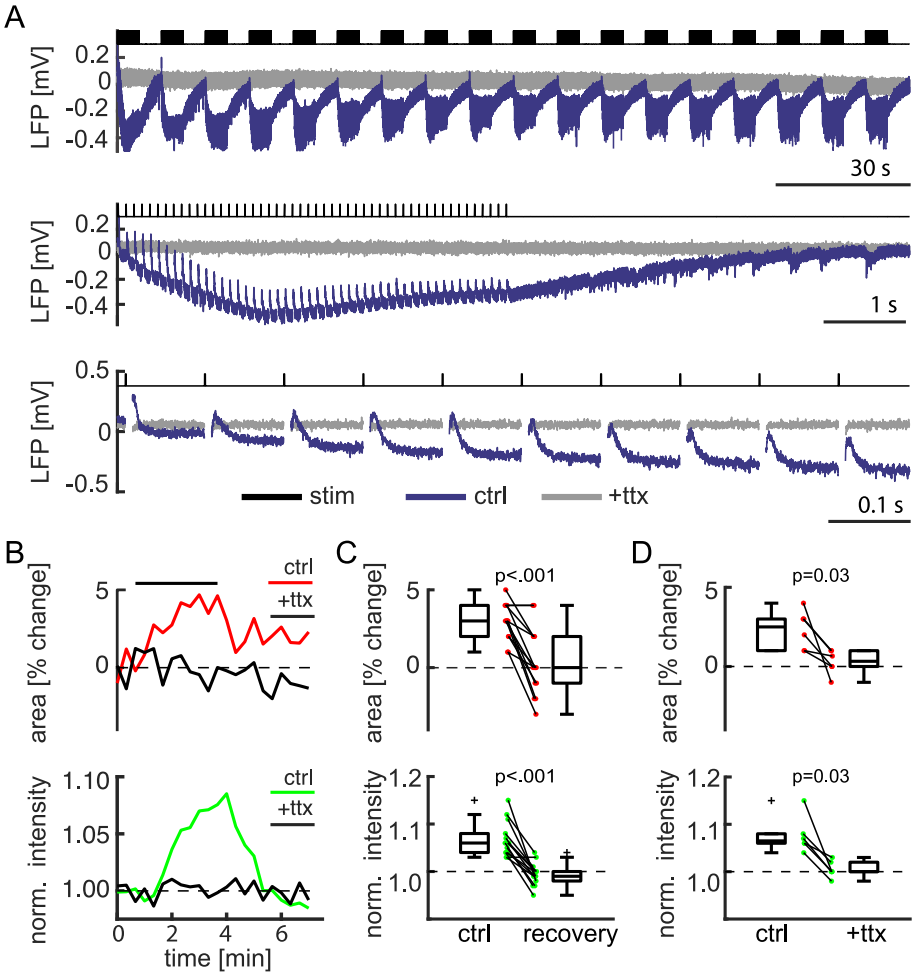

Fig. 4. Stimulation-induced Fluo accumulation and swelling of astrocytes.
A) Local field potential (LFP) recording (gray and blue) during stimulation (18 bursts given at 0.1 Hz, each burst consisting of 50 stimuli given at 10 Hz). Top, full-length stimulation series; middle, first burst; bottom, first 10 stimuli of first burst. Stim (topmost trace, black) indicates stimulation; light and dark gray, LFP during stimulation in aCSF with and without 1 μM tetrodotoxin (ttx), respectively. Stimulation artifacts were cut out for clarity.
B) Exemplary graphs of self-normalized astrocytic area (top) and Fluo intensity (bottom, both: mean of 3 astrocytes from one recording) during stimulation (black bar). The slice was either perfused with aCSF (ctrl, red and green traces) or with aCSF containing 1 μM ttx (black traces).
C) Boxplots summarizing maximal astrocytic area (top) and Fluo intensity (bottom) during stimulation and after 3 min of recovery (each normalized to the pre-stimulation baseline; $n = 14$ stimulation series, 12 slices, 5 mice, Wilcoxon test). Individual values represent averages from 3 astrocytes and 3 consecutive timepoints for each condition.
D) Boxplots summarizing maximal astrocytic area (top) and Fluo intensity (bottom) during stimulation normalized to the pre-stimulation baseline. Slices were perfused with aCSF ('ctrl') or aCSF containing ttx ('+ttx', 0.5–1 μM). Data of 0.5 μM and 1 μM ttx were pooled (each concentration: n = 3 slices, 2 mice, Wilcoxon test). (For interpretation of the references to colour in this figure legend, the reader is referred to the web version of this article.)

increased astrocytic area from 122% (116, 127) to 135% (130, 150) ($n = 12$ slices, 5 mice, $p < 0.001$ and $p = 0.006$, respectively, Wilcoxon test, Fig. 3F,G). Fig. 3F illustrates the rapid reduction of astrocytic Fluo intensity by additional glutamate in presence of 10 mM $[K^+]_o$.

3.6. Electrical stimulation induces astrocytic Fluo accumulation

In acute brain slices, electrical stimulation of neuronal activity has been associated with transient elevations of $[K^+]_o$ (although lower than during SDs) (Larsen and MacAulay, 2017; Berndt et al., 2020) and glutamate (Dulla et al., 2008; Brandner et al., 2022). Given our results so far, astrocytic Fluo intensity should increase due to elevated $[K^+]_o$ but decrease due to elevated glutamate. We therefore tested, how electrical stimulation affects astrocytic Fluo intensity and also measured the astrocyte-covered area. We made use of repetitive burst stimulation (50 stimuli at 10 Hz/burst, 1 burst/10 s), which induced stimulus-associated population-spike responses (Fig. 4A, bottom), and additive burst-associated negative DC-potential deflections (Fig. 4A). As expected population-spikes and DC-deflections were blocked by ttx (0.5–1 µM, Fig. 4A). During stimulation astrocytic Fluo intensity increased by factor 1.06 (1.04, 1.08) and the area increased by 3% (2, 4), respectively, and returned to 0.99 (0.98, 1.00) and 100% (99, 102) 3 min post stimulation

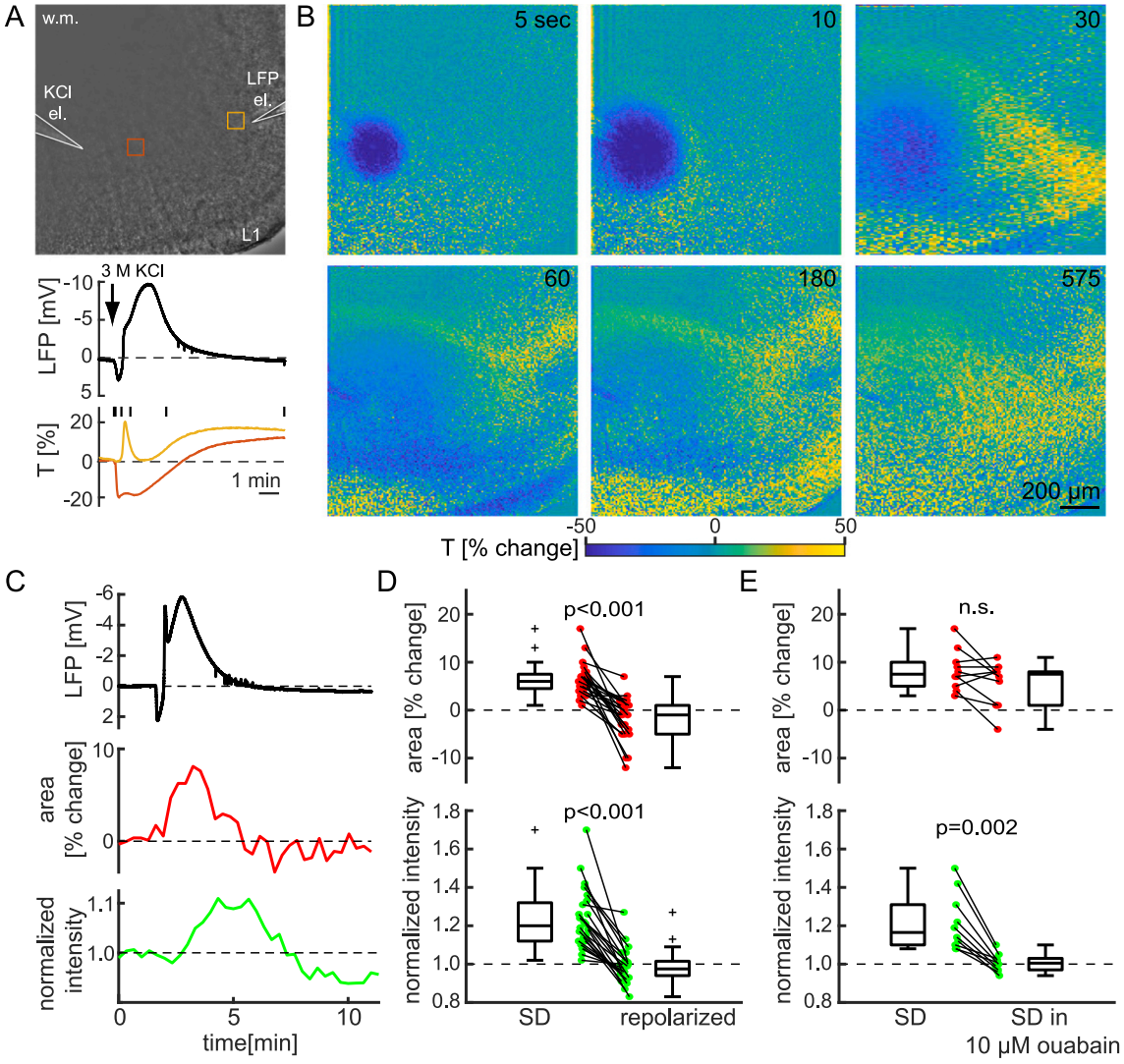

Fig. 5. Astrocytic accumulation of Fluo and swelling during SDs.

A) Top, transmission image of a neocortical slice. Glass microelectrodes for puff application of 3 M KCl to induce an SD ('KCl-el.') and for recording the local field potential ('LFP-el.') are outlined (white lines). White matter ('w.m.') and layer 1 ('L1') are labeled to indicate slice orientation. Yellow and orange rectangles indicate regions from which the time-dependent optical transmission was quantified. Bottom, LFP and transmission for the yellow and orange rectangles during an SD evoked by puff-application of KCl. Short vertical lines indicate time points at which the images displayed in B were taken.

B) Digital subtraction images of transmission at different time points (indicated in each top right corner) during and after an SD. The last image prior to KCl puff application was subtracted from each subsequent image and the differences were expressed as a percentage of the absolute transmission prior to SD. Based on the wavefront of the transmission change, the SD was calculated to have propagated at 2.7 mm/min.

C) LFP (top), and self-normalized area and Fluo intensity (middle and bottom, mean of 3 astrocytes) during an SD evoked by puff-application of KCl in a SR-101 and Fluo stained slice.

D) Boxplots summarizing astrocytic area (top) and Fluo intensity (bottom) during SDs and after repolarization, each normalized to the average of 3 consecutive pre-SD timepoints ($n = 24$ SDs, 19 slices, 10 mice, Wilcoxon test). Individual points are averages of 3 astrocytes from the same brain slice.

E) Boxplots as in D summarizing SD-associated changes of astrocytic area and Fluo intensity in standard aCSF ('SD') and in aCSF with addition of ouabain ('SD in 10 µM ouabain'; n = 10 paired SDs, 10 slices, 6 mice). Note that ouabain prevented astrocytic Fluo accumulation, whereas swelling was not consistently affected. (For interpretation of the references to colour in this figure legend, the reader is referred to the web version of this article.)

($n = 14$ stimulation series, 12 slices, 5 mice, both: $p < 0.001$, Wilcoxon test). Of note, the observed changes in Fluo intensity and area were about 7 times smaller than during wash in of 10 mM $[K^+]_o$. Astrocytic Fluo accumulation and swelling were prevented by ttx (Fig. 4D).

3.7. SDs induce Na/K-ATPase dependent Fluo accumulation

Our incidental observation that astrocytes take up Fluo during SDs was made in a model that relies on 'global' $[K^+]_o$ elevation by washin of aCSF containing 20 mM KCl. This leaves open the question if SDs themselves, when triggered focally and remotely, lead to similar astrocytic Fluo accumulation. As reported previously (Reiffurth et al., 2020), puff-induced SDs (KCl (3 M) by microelectrode) showed a negative deflection of the DC potential (up to 10 mV, Fig. 5A,C) and changes in light transmission with centrifugal propagation (Fig. 5B). The monochromatic (800 nm) light transmission patterns were different in vicinity of the SD induction site compared with more remote sites (e.g. near the LFP electrode, Fig. 5A,B). Near the induction site, SD began with a rapid reduction, whereas more remotely, SD began with a transient increase in transmission (Fig. 5A,B, representative of 11 SDs in 5 slices from 3 mice). Confirming SD-associated astrocytic swelling (Risher et al., 2012), we found that astrocytic area intensity increased by 6% (5, 8) during SD and normalized to 99% (95, 101) after repolarization ($n = 24$ SDs, 19 slices, 10 mice, $p < 0.001$, Wilcoxon test, Fig. 5C,D). In parallel, Fluo intensity increased by factor 1.20 (1.12, 1.32) during SD, and returned to 0.98 (0.94, 1.02) after repolarization ($n = 24$ SDs, 19 slices, 10 mice, $p < 0.001$, Wilcoxon test, Fig. 5C,D). In presence of ouabain (10 μM), Fluo intensity during SD was reduced from factor 1.17 (1.10, 1.31) to 1.01 (0.97, 1.03) ($n = 10$ SDs, 10 slices, 6 mice, $p = 0.002$, Wilcoxon test), whereas astrocytic swelling was reduced in some slices but not at the group level (Fig. 5E). Puffs that failed to induce SDs were not followed by increased astrocytic Fluo intensity. To summarize, astrocytic Fluo accumulation is a marker of SD, is sensitive to NaK-ATPase inhibition, and is not a sufficient marker for SD-associated swelling.

4. Discussion

In the present study, we investigated previously unknown astrocytic dynamics of Fluo, which we incidentally found during K^+-induced SDs in acute mouse brain slices. We report that accumulation of Fluo by astrocytes is: a) dose-dependent on $[K^+]_o$ and increases in parallel with astrocytic swelling, b) not a ubiquitous marker of astrocytic swelling, c) reduced by extracellular glutamate, d) suppressed by Na/K-ATPase inhibition and low $[Na^+]_o$, e) triggered by neuronal activity, and f) triggered by SD.

Astrocytes were labeled by SR-101, which has been shown to additionally label a proportion of hippocampal and cortical oligodendrocytes in vitro (Wasseff and Scherer, 2011; Hagos and Hülsmann, 2016) and in the neocortex in vivo (Hill and Grutzendler, 2014). Therefore, we cannot rule out that some SR-101 positive cells were oligodendrocytes. However, in-vivo, astrocytes made up the majority of SR-101 positive cells (~60–90% depending on cortical depths) (Hill and Grutzendler, 2014) and were the more numerous cell type in vitro (Wasseff and Scherer, 2011; Hagos and Hülsmann, 2016). A study that characterized SR-101-positive cells in vitro in acute hippocampal brain slices by electrophysiology found a low membrane resistance (~10 MΩ), which is characteristic for astrocytes (Kafitz et al., 2008) and which is much lower than the membrane resistance of white matter oligodendrocytes (~380 MΩ) (Bakiri et al., 2011). Furthermore, elevated $[K^+]_o$ was shown to cause astrocyte-selective swelling (Walch et al., 2020), an observation that has not been made for oligodendrocytes. Taken together, these studies provide evidence that our observations were predominantly made in astrocytes, but we cannot formally exclude that some oligodendrocytes were included in the analysis.

Consistent with previous studies, elevated $[K^+]_o$, elevated extracellular glutamate and hypoosmotic extracellular solution induced swelling of astrocytes (Hansson et al., 2000; Hirrlinger et al., 2008; Risher et al., 2009; Florence et al., 2012; Larsen and MacAulay, 2017; Shi et al., 2017; Walch et al., 2020). Among these three triggers of swelling, only elevated $[K^+]_o$ was associated with a parallel increase in astrocytic Fluo intensity. The mechanisms that link $[K^+]_o$ and astrocytic swelling remain incompletely understood. Buffering of $[K^+]_o$ has been attributed to the function of astrocytes and was suggested to involve inter alia Kir4.1 channels and the Na/K-ATPase (Larsen and MacAulay, 2014; Larsen et al., 2016). Of note, inhibition of the Na/K-ATPase prevented K^+-induced astrocytic swelling in cell culture (Walz and Hinks, 1985) and in acute mouse brain slices (Walch et al., 2020), which we confirmed. In addition, we found that Na/K-ATPase inhibition by ouabain or digoxin blocked astrocytic Fluo accumulation. At the applied concentration of 10 μM, ouabain is expected to block most of the astrocytic α2-isoform of the Na/K-ATPase, while only a partial block is expected for the more generally expressed α1-isoform, which has a ~ 1000 fold higher IC50 (~50 μM) (O'brien et al., 1994; Moseley et al., 2003). Acute elevation of $[K^+]_o$ increased Na/K-ATPase activity in cultured mouse astrocytes (Hajek et al., 1996), however with its stoichiometry – uptake of 2 K^+ ions in exchange for 3 Na^+ ions – Na/K-ATPase by itself cannot cause astrocytic swelling. We saw that a reduction in $[Na^+]_o$ likewise blocked Fluo accumulation and swelling, which suggests that Na^+ gradients established by the Na/K-ATPase drive secondary active transport of Fluo, e.g. via Na^+-coupled uptake of glutamate by EAATs (Verkhratsky and Nedergaard, 2018). Glutamate is released from excitatory neurons during action potential firing, and action potential frequency was shown to increase at $[K^+]_o$ of 10.5 mM (Walch et al., 2020). Astrocytes are known to buffer excess glutamate by uptake via EAATs (Verkhratsky and Nedergaard, 2018). However, blocking EAATs did not prevent Fluo accumulation at 10 mM $[K^+]_o$. We thus have no evidence that Fluo is a substrate of EAATs. Inhibition of EAATs supposedly elevates extracellular glutamate, however, direct glutamate application in presence of 10 mM $[K^+]_o$ lowered astrocytic Fluo compared with wash in of 10 mM $[K^+]_o$ alone. This implies that the Fluo lowering effect of extracellular glutamate depends on its uptake into astrocytes. Na^+-coupled uptake of glutamate by EAATs has been shown to increase intracellular Na^+ (Langer and Rose, 2009). Thereby transmembrane Na^+ gradients are reduced, which may in turn reduce the driving force for other Na^+-coupled transporters, including one for Fluo. Alternatively, our data supports uptake of glutamate in exchange for Fluo or its physiological substrate.

While accumulation of Fluo depended on Na/K-ATPase activity and was opposed by extracellular glutamate, we were not able to identify the specific transport mechanism of Fluo. Astrocytic Fluo accumulation and swelling were not prevented by inhibition of NBCe-1 with S0857 in our experiments, although NBCe-1 inhibition by DIDS was previously reported to reduce $[K^+]_o$-induced swelling of astrocytes (Florence et al., 2012) and partially prevented the activity-dependent reduction in extracellular space volume that was attributed to astrocytic swelling (Larsen and MacAulay, 2017). In contrast, Walch et al. (2020) found no effect of DIDS on $[K^+]_o$-induced swelling in acute slices from C57Bl6 mice after 5 min of exposure to 10.5 mM $[K^+]_o$. Since DIDS is a fluorescent compound that interferes with the Fluo signal, we could not use it to measure Fluo kinetics. The differing results for NBCe-1 mediated astrocytic swelling are discussed in greater detail in a recent review article (Walch and Fiacco, 2022). Inhibition of MCTs by phloretin or 4-CIN did not reduce astrocytic Fluo accumulation and swelling, although release of lactate was shown to depend on $[K^+]_o$ in vitro and was associated with elevated $[K^+]_o$ in vivo in mice (Sotelo-Hitschfeld et al., 2015). Release of lactate may cause compensatory uptake of other anions (e.g. Fluo) to maintain electroneutrality. Elevated $[K^+]_o$ has been shown to activate astrocytic glycolysis (in organotypic hippocampal slices and cultured astrocytes) and bidirectional glucose transport via Glut-1 (in cultured astrocytes) (Ruminot et al., 2011; Köhler et al., 2018; Fernández-Moncada et al., 2021). Glut-1 passively transports water

(Stokum et al., 2016). We thus asked whether Glut-1 also transports Fluo and found that inhibition of Glut-1 by cytochalasin B had no effect on K^+-induced astrocytic Fluo accumulation and volume changes. Likewise, we saw no effect by inhibition of OATPs, which are expressed in astrocytes (Verkhratsky and Nedergaard, 2018) and have been shown to transport Fluo into human and rat hepatocytes (De Bruyn et al., 2011) and into insect cells that express human OATPs (Patik et al., 2015). We further tested if Fluo is released from astrocytes through VRACs, which open when cells swell (Osei-Owusu et al., 2018) and found no evidence thereof. Fluo release via VRACs would have indicated different transport mechanisms of Fluo *uptake* versus *release*.

As yet another mechanistic target, we investigated if Fluo accumulation is secondarily coupled to astrocytic buffering of $[K^+]_o$ via Kir4.1 channels (Larsen and MacAulay, 2014), although Kir4.1 channels themselves are not expected to be permeable for larger and negatively charged Fluo molecules. However, we found no evidence for a role of Kir4.1 channels, because their inhibition by 100 μM $BaCl_2$ did not prevent astrocytic Fluo accumulation. Similarly, astrocytic swelling induced by elevated $[K^+]_o$ was not affected by 100 μM $BaCl_2$, which has been demonstrated previously (Walch et al., 2020) and is supported by another study that found no difference in the volumetric changes of the extracellular space when K^+ was ionophoretically applied without or in presence of Ba^{2+} (Jauch et al., 2002).

Elevated $[K^+]_o$ as well as elevated extracellular glutamate led to swelling of astrocytes, yet the effect on astrocytic Fluo accumulation was oppositional. $[K^+]_o$ has been shown to rise to ceiling levels of 10–12 mM during electrical stimulation in vivo in cats and in rat hippocampal slices (Heinemann and Dieter Lux, 1977; Larsen and MacAulay, 2017). Quantitative data on activity-dependent changes of extracellular glutamate concentrations are sparse. Increases by 15 μM after high frequency electrical stimulation (100 Hz) were measured in mouse hippocampal slices (Ikegami et al., 2014), yet, higher concentrations of ~1 mM may be reached in the synaptic cleft (Clements et al., 1992). We saw astrocytic Fluo accumulation and swelling during electrical stimulation, which implies that $[K^+]_o$-induced Fluo uptake outweighed glutamate-induced efflux. $[K^+]_o$-induced swelling of astrocytic endfeet has been proposed as mechanism that regulates activity-dependent perivascular glymphatic flow (Hablitz and Nedergaard, 2021). According to our data this process may involve accumulation of anions and can be visualized by Fluo imaging. To rule out direct effects of astrocytic stimulation, action potential propagation was blocked by ttx. This prevented astrocytic Fluo accumulation, which supports signalling from neurons to astrocytes, presumably release of K^+, to underlie astrocytic Fluo dynamics.

Similar to electrical stimulation of neuronal activity, both elevations of $[K^+]_o$ (up to ~80 mM) and of extracellular glutamate were recorded during SDs (Dreier et al., 2018; Menyhárt et al., 2022). We saw astrocytic Fluo accumulation and swelling during focally induced SDs, which, as during electrical stimulation, indicates a predominant effect of $[K^+]_o$-induced accumulation of Fluo over glutamate-induced efflux. We further found that ouabain prevented astrocytic Fluo accumulation during SDs. While some slices showed reduced astrocytic swelling, there was no significant reduction by ouabain at the group level. This suggests that astrocytic Fluo accumulation is strictly Na/K-ATPase dependent, whereas swelling during SD is in part caused by different mechanisms, e.g. swelling induced by glutamate and by Gibbs-Donnan forces. Gibbs-Donnan forces are created mainly by the high concentration of negatively charged intracellular proteins that attract small solutes and water. Under physiological conditions Gibbs-Donnan forces are balanced by the high concentration of $[Na^+]_o$ (maintained by the Na/K-ATPase), which similarly attracts water. This state is referred to as the double Gibbs-Donnan state (Dreier et al., 2013; Lemale et al., 2022). During SD, $[Na^+]_o$ falls from ~150 mM to ~60 mM due to influx of Na^+ into neurons, and, depending on the availability of ATP, due to reduced Na/K-ATPase activity. This causes a shift from the double Gibbs-Donnan state towards the simple Gibbs-Donnan equilibrium, where the Gibbs-Donnan forces are no longer balanced by $[Na^+]_o$ resulting in swelling of cells during SD (Dreier et al., 2013; Lemale et al., 2022). Swelling due to Gibbs-Donnan forces reverses by activity of the Na/K-ATPase, which explains why ouabain could not prevent this component of swelling. Ouabain by itself did not aggravate swelling because the dosage was chosen to inhibit predominantly the astrocytic α2-isoform and not the 'housekeeping' α1-isoform (see §3 of the discussion and (O'brien et al., 1994; Moseley et al., 2003)). The increase in Fluo signal in astrocytes indicates the accumulation of anions in astrocytes and can thereby help to identify fluxes of anions during SD, which are not well understood (Dreier et al., 2018).

4.1. Conclusions and future perspectives

Astrocytic endfeet ensheath parenchymal brain vessels, synapses and form the glia limitans at the pia mater (Abbott et al., 2006). Therefore, astrocytes are a key element of the glymphatic system (Hablitz and Nedergaard, 2021) connecting cerebrospinal fluid, interstitial fluid and blood vessels. Fluo may be used as a marker to visualize anion fluxes during $[K^+]_o$ but not glutamate-induced or osmotic astrocytic swelling. Understanding the mechanisms of $[K^+]_o$-dependent astrocytic Fluo dynamics promises novel insights into anion and fluid movements between different compartments of the brain during physiological neuronal activity, pathological network activity, e.g. epileptic seizures and SDs, and during formation and regression of cerebral edema.

4.2. Limitations

All experiments of this study were performed in vitro, i.e. in absence of intracranial pressure and blood flood, and the extravascular fluid compartment is greatly enlarged in brain slice experiments. Pharmacological experiments can be affected by reduced target specificity or distribution kinetics within the limited wash in period. SR-101 has been shown to label oligodendrocytes in addition to astrocytes in acute cortical and hippocampal slices in mice (Wasseff and Scherer, 2011; Hagos and Hülsmann, 2016).

Supplementary data to this article can be found online at https://doi.org/10.1016/j.nbd.2023.106026.

Source of funding

This research was supported by the Deutsche Forschungsgemeinschaft (HI1414/7-1).

CRediT authorship contribution statement

Karl Schoknecht: Conceptualization, Investigation, Formal analysis, Writing - original draft, Writing - review & editing. **Johannes Hirrlinger:** Conceptualization, Writing – review & editing. **Jens Eilers:** Conceptualization, Writing – review & editing.

Declaration of Competing Interest

The authors declare no conflict of interest.

Data availability

Data will be made available on request.

Acknowledgement

The authors would like to thank Gudrun Bethge for technical assistance and Profs. Jens Dreier and Alon Friedman for helpful discussions. The publication costs were funded by the Open Access Publishing Fund of Leipzig University supported by the German Research Foundation within the program Open Access Publication Funding.

References

Abbott, N.J., Rönnbäck, L., Hansson, E., 2006. Astrocyte-endothelial interactions at the blood-brain barrier. Nat. Rev. Neurosci. 7, 41–53.

Bakiri, Y., Káradóttir, R., Cossell, L., Attwell, D., 2011. Morphological and electrical properties of oligodendrocytes in the white matter of the corpus callosum and cerebellum. J. Physiol. 589, 559–573.

Berndt, N., Kovács, R., Rösner, J., Wallach, I., Dreier, J.P., Liotta, A., 2020. Flavin adenine dinucleotide fluorescence as an early marker of mitochondrial impairment during brain hypoxia. Int. J. Mol. Sci. 21.

Brandner, S., Aicher, S., Schroeter, S., Swierzy, I., Kinfe, T.M., Buchfelder, M., Maslarova, A., Stadlbauer, A., 2022. Real-time imaging of glutamate transients in the extracellular space of acute human brain slices using a single-wavelength glutamate fluorescence nanosensor. Sci. Rep. 12, 1–10.

Clements, J.D., Lester, R.A.J., Tong, G., Jahr, C.E., Westbrook, G.L., 1992. The time course of glutamate in the synaptic cleft. Science 258, 1498–1501.

De Bruyn, T., Fattah, S., Stieger, B., Augustijns, P., Annaert, P., 2011. Sodium fluorescein is a probe substrate for hepatic drug transport mediated by OATP1B1 and OATP1B3. J. Pharm. Sci. 100, 5018–5030.

Dreier, J.P., Reiffurth, C., 2015. The stroke-migraine depolarization continuum. Neuron 86, 902–922.

Dreier, J.P., Isele, T., Reiffurth, C., Offenhauser, N., Kirov, S.A., Dahlem, M.A., Herreras, O., 2013. Is spreading depolarization characterized by an abrupt, massive release of gibbs free energy from the human brain cortex? Neuroscientist 19, 25–42.

Dreier, J.P., et al., 2017. Recording, analysis, and interpretation of spreading depolarizations in neurointensive care: review and recommendations of the COSBID research group. J. Cereb. Blood Flow Metab. 37, 1595–1625.

Dreier, J.P., Lemale, C.L., Kola, V., Friedman, A., Schoknecht, K., 2018. Spreading depolarization is not an epiphenomenon but the principal mechanism of the cytotoxic edema in various gray matter structures of the brain during stroke. Neuropharmacology 134, 189–207.

Dulla, C., Tani, H., Okumoto, S., Frommer, W.B., Reimer, R.J., Huguenard, J.R., 2008. Imaging of glutamate in brain slices using FRET sensors. J. Neurosci. Methods 168, 306–319.

Fernández-Moncada, I., Robles-Maldonado, D., Castro, P., Alegría, K., Epp, R., Ruminot, I., Barros, L.F., 2021. Bidirectional astrocytic GLUT1 activation by elevated extracellular K^+. Glia 69, 1012–1021.

Florence, C.M., Baillie, L.D., Mulligan, S.J., 2012. Dynamic volume changes in astrocytes are an intrinsic phenomenon mediated by bicarbonate ion flux. PLoS One 7, 1–9.

Guizar-Sicairos, M., Thurman, S.T., Fienup, J.R., 2008. Efficient subpixel image registration algorithms. Opt. Lett. 33, 156.

Gursoy-Ozdemir, Y., Qiu, J., Matsuoka, N., Bolay, H., Bermpohl, D., Jin, H., Wang, X., Rosenberg, G.A., Lo, E.H., Moskowitz, M.A., 2004. Cortical spreading depression activates and upregulates MMP-9. J. Clin. Invest. 113, 1447–1455.

Hablitz, L.M., Nedergaard, M., 2021. The glymphatic system: a novel component of fundamental neurobiology. J. Neurosci. 41, 7698–7711.

Hagos, L., Hülsmann, S., 2016. Unspecific labelling of oligodendrocytes by sulforhodamine 101 depends on astrocytic uptake via the thyroid hormone transporter OATP1C1 (SLCO1C1). Neurosci. Lett. 631, 13–18.

Hajek, I., Subbarao, K.V.S., Hertz, L., 1996. Acute and chronic effects of potassium and noradrenaline on Na^+, K^+-ATPase activity in cultured mouse neurons and astrocytes. Neurochem. Int. 28, 335–342.

Hansson, E., Muyderman, H., Leonova, J., Allansson, L., Sinclair, J., Blomstrand, F., Thorlin, T., Nilsson, M., Rönnbäck, L., 2000. Astroglia and glutamate in physiology and pathology: aspects on glutamate transport, glutamate-induced cell swelling and gap-junction communication. Neurochem. Int. 37, 317–329.

Heinemann, U., Dieter Lux, H., 1977. Ceiling of stimulus induced rises in extracellular potassium concentration in the cerebral cortex of cat. Brain Res. 120, 231–249.

Hill, R.A., Grutzendler, J., 2014. In vivo imaging of oligodendrocytes with sulforhodamine 101. Nat. Methods 11, 1081–1082.

Hirrlinger, P.G., Wurm, A., Hirrlinger, J., Bringmann, A., Reichenbach, A., 2008. Osmotic swelling characteristics of glial cells in the murine hippocampus, cerebellum, and retina in situ. J. Neurochem. 105, 1405–1417.

Ikegami, Y., Hozumi, S., Shoji, A., Hirano-Iwata, A., Bliss, T., Sugawara, M., 2014. Real-time monitoring of extracellular l-glutamate levels released by high-frequency stimulation at region CA1 of hippocampal slices with a glass capillary-based l-glutamate sensor. Sens Bio-Sensing Res 2, 31–37.

Jauch, R., Windmüller, O., Lehmann, T.N., Heinemann, U., Gabriel, S., 2002. Effects of barium, furosemide, ouabaine and 4,4′-diisothiocyanatostilbene-2,2′-disulfonic acid (DIDS) on ionophoretically-induced changes in extracellular potassium concentration in hippocampal slices from rats and from patients with epilepsy. Brain Res. 925, 18–27.

Kafitz, K.W., Meier, S.D., Stephan, J., Rose, C.R., 2008. Developmental profile and properties of sulforhodamine 101-labeled glial cells in acute brain slices of rat hippocampus. J. Neurosci. Methods 169, 84–92.

Köhler, S., Winkler, U., Sicker, M., Hirrlinger, J., 2018. NBCe1 mediates the regulation of the NADH/NAD^+ redox state in cortical astrocytes by neuronal signals. Glia 66, 2233–2245.

Langer, J., Rose, C.R., 2009. Synaptically induced sodium signals in hippocampal astrocytes in situ. J. Physiol. 587, 5859–5877.

Larsen, B.R., MacAulay, N., 2014. Kir4.1-mediated spatial buffering of K. Channels (Austin) 8, 544–550.

Larsen, B.R., MacAulay, N., 2017. Activity-dependent astrocyte swelling is mediated by pH-regulating mechanisms. Glia 65, 1668–1681.

Larsen, B.R., Stoica, A., MacAulay, N., 2016. Managing brain extracellular K^+ during neuronal activity: the physiological role of the Na^+/K^+-ATPase subunit isoforms. Front. Physiol. 7, 1–10.

Lemale, C.L., Lückl, J., Horst, V., Reiffurth, C., Major, S., Hecht, N., Woitzik, J., Dreier, J. P., 2022. Migraine aura, transient ischemic attacks, stroke, and dying of the brain share the same key pathophysiological process in neurons driven by gibbs–donnan forces, namely spreading depolarization. Front. Cell. Neurosci. 16, 1–29.

Madisen, L., Zwingman, T.A., Sunkin, S.M., Oh, S.W., Zariwala, H.A., Gu, H., Ng, L.L., Palmiter, R.D., Hawrylycz, M.J., Jones, A.R., Lein, E.S., Zeng, H., 2010. A robust and high-throughput Cre reporting and characterization system for the whole mouse brain. Nat. Neurosci. 13, 133–140.

Menyhárt, Á., Frank, R., Farkas, A.E., Süle, Z., Varga, V., Nyúl-Tóth, Á., Meiller, A., Ivánkovits-Kiss, O., Lemale, C.L., Szabó, Í., Tóth, R., Zölei-Szénási, D., Woitzik, J., Marinesco, S., Krizbai, I.A., Bari, F., Dreier, J.P., Farkas, E., 2022. Malignant astrocyte swelling and impaired glutamate clearance drive the expansion of injurious spreading depolarization foci. J. Cereb. Blood Flow Metab. 42, 584–599.

Moseley, A.E., Lieske, S.P., Wetzel, R.K., James, P.F., He, S., Shelly, D.A., Paul, R.J., Boivin, G.P., Witte, D.P., Ramirez, J.M., Sweadner, K.J., Lingrel, J.B., 2003. The Na, K-ATPase α2 isoform is expressed in neurons, and its absence disrupts neuronal activity in newborn mice. J. Biol. Chem. 278, 5317–5324.

O'brien, W.J., Lingrel, J.B., Wallick, E.T., 1994. Ouabain binding kinetics of the rat alpha two and alpha three isoforms of the sodium-potassium adenosine triphosphate. Arch. Biochem. Biophys. 310, 32–39.

Osei-Owusu, J., Yang, J., Vitery, M.C., Qiu, Z., 2018. Molecular biology and physiology of volume-regulated Anion Channel (VRAC). Curr. Top. Membr. 81, 177–203.

Parker, E., et al., 2022. Concussion susceptibility is mediated by spreading depolarization-induced neurovascular dysfunction. Brain 145, 2049–2063.

Patik, I., Kovacsics, D., Német, O., Gera, M., Várady, G., Stieger, B., Hagenbuch, B., Szakács, G., Özvegy-Laczka, C., 2015. Functional expression of the 11 human organic anion transporting polypeptides in insect cells reveals that sodium fluorescein is a general OATP substrate. Biochem. Pharmacol. 98, 649–658.

Reiffurth, C., Alam, M., Zahedi-Khorasani, M., Major, S., Dreier, J.P., 2020. Na^+/K^+-ATPase α isoform deficiency results in distinct spreading depolarization phenotypes. J Cereb Blood Flow Metab. 40 (3), 622–638.

Risher, W.C., Andrew, R.D., Kirov, S.A., 2009. Real-time passive volume responses of astrocytes to acute osmotic and ischemic stress in cortical slices and in vivo revealed by two-photon microscopy. Glia 57, 207–221.

Risher, W.C., Croom, D., Kirov, S.A., 2012. Persistent astroglial swelling accompanies rapid reversible dendritic injury during stroke-induced spreading depolarizations. Glia 60, 1709–1720.

Ruminot, I., Gutiérrez, R., Peña-Münzenmayer, G., Añazco, C., Sotelo-Hitschfeld, T., Lerchundi, R., Niemeyer, M.I., Shull, G.E., Barros, L.F., 2011. NBCe1 mediates the acute stimulation of astrocytic glycolysis by extracellular K^+. J. Neurosci. 31, 14264–14271.

Sadeghian, H., Lacoste, B., Qin, T., Toussay, X., Rosa, R., Oka, F., Chung, D.Y., Takizawa, T., Gu, C., Ayata, C., 2018. Spreading depolarizations trigger caveolin-1-dependent endothelial transcytosis. Ann. Neurol. 84, 409–423.

Schoknecht, K., Prager, O., Vazana, U., Kamintsky, L., Harhausen, D., Zille, M., Figge, L., Chassidim, Y., Schellenberger, E., Kovács, R., Heinemann, U., Friedman, A., 2014. Monitoring stroke progression: *in vivo* imaging of cortical perfusion, blood—brain barrier permeability and cellular damage in the rat photothrombosis model. J. Cereb. Blood Flow Metab. 34, 1791–1801.

Shaner, N.C., Campbell, R.E., Steinbach, P.A., Giepmans, B.N.G., Palmer, A.E., Tsien, R. Y., 2004. Improved monomeric red, orange and yellow fluorescent proteins derived from Discosoma sp. red fluorescent protein. Nat. Biotechnol. 22, 1567–1572.

Shi, Z., Zhang, W., Lu, Y., Lu, Y., Xu, L., Fang, Q., Wu, M., Jia, M., Wang, Y., Dong, L., Yan, X., Yang, S., Yuan, F., 2017. Aquaporin 4-mediated glutamate-induced astrocyte swelling is partially mediated through metabotropic glutamate receptor 5 activation. Front. Cell. Neurosci. 11, 1–12.

Sotelo-Hitschfeld, T., et al., 2015. Channel-mediated lactate release by K^+-stimulated astrocytes. J. Neurosci. 35, 4168–4178.

Stokum, J.A., Gerzanich, V., Simard, J.M., 2016. Molecular pathophysiology of cerebral edema. J. Cereb. Blood Flow Metab. 36, 513–538.

Verkhratsky, A., Nedergaard, M., 2018. Physiology of astroglia. Physiol. Rev. 98, 239–389.

Walch, E., Fiacco, T.A., 2022. Honey, I shrunk the extracellular space: measurements and mechanisms of astrocyte swelling. Glia 1–19.

Walch, E., Murphy, T.R., Cuvelier, N., Aldoghmi, M., Morozova, C., Donohue, J., Young, G., Samant, A., Garcia, S., Alvarez, C., Bilas, A., Davila, D., Binder, D.K., Fiacco, T.A., 2020. Astrocyte-selective volume increase in elevated extracellular potassium conditions is mediated by the Na+/K+ ATPase and occurs independently of aquaporin 4. ASN Neuro 12.

Walz, W., Hinks, E.C., 1985. Carrier-mediated KCl accumulation accompanied by water movements is involved in the control of physiological K^+ levels by astrocytes. Brain Res. 343, 44–51.

Wasseff, S.K., Scherer, S.S., 2011. Cx32 and Cx47 mediate oligodendrocyte:astrocyte and oligodendrocyte:oligodendrocyte gap junction coupling. Neurobiol. Dis. 42, 506–513.

Zhou, N., Gordon, G.R.J., Feighan, D., MacVicar, B.A., 2010. Transient swelling, acidification, and mitochondrial depolarization occurs in neurons but not astrocytes during spreading depression. Cereb. Cortex 20, 2614–2624.